

Submitted: 14/05/2024

Accepted: 11/07/2024

Published: 31/08/2024

Imaging of a subcutaneous abscessation in the back of a calf with hindlimb paralysis

Takeshi Tsuka^{1*} , Noriyo Usaki² , Midori Hatanaka² , Yusuke Murahata¹ , Takashi Takeuchi¹ , Yuji Sunden¹ , Takehito Morita¹ , Yoshiharu Okamoto³ , Miyuu Tanaka⁴ , Takeshi Izawa⁴ , Mitsuru Kuwamura⁴  and Norio Yamagishi⁴ 

¹Department of Veterinary Clinical Medicine, Joint Department of Veterinary Medicine, Faculty of Agriculture, Tottori University, Tottori, Japan

²Hyogo Prefectural Federation Agricultural Mutual Aid Association, Kobe, Japan

³WOLVES HAND Advanced Veterinary Medical Research Institute, Osaka, Japan

⁴Graduate School of Veterinary Science, Osaka Metropolitan University, Osaka, Japan

ABSTRACT

Background: Ultrasonography is not chosen as the common imaging modality to diagnose spinal cord diseases. The present report indicates good diagnostic efficacy of ultrasonography for identifying spinal cord compressed by subcutaneous mass when scanning through the defected vertebral laminae and spinous process.

Case Description: A five-month-old female Holstein calf presented with progressive hindlimb paralysis following a surgical resection of a back mass conducted at 21 days of age. The mass was subsequently histopathologically diagnosed as a pulmonary choristoma. Alongside hindlimb paralysis, the calf developed a swollen back at the lumbar region where the mass was removed. This suggested regrowth of the resected mass, causing injury to the underlying spinal cord. Ultrasonography identified the subcutaneous involvement of the capsular mass, which had three anechoic cavities separated by the echogenic septal structures. The spinal cord could be ultrasonographically demonstrated as adjacent to the mass through the defected vertebral laminae and spinous process in the second and third lumbar vertebrae. Ultrasound-guided centesis allowed the collection of purulent exudates in which *Escherichia coli* was isolated. Myelography and subsequent computed tomography (CT) revealed a partial blockage of the intradural flow of contrast media at the levels of the second and third lumbar vertebrae, diagnosed as spina bifida on the CT images. When applying ultrasonography to the spinal cord within a saline pool soon after the subcutaneous abscess was successfully resected, the spinal cord was characterized by the interrupted and partly extended hyperechogenic line of the central canal within the echogenic parenchyma. The echotexture of the spinal cord showed damage due to compression from the subcutaneous abscess. The animal had a sub-optimal postoperative outcome, including limited improvement of the neurological signs.

Conclusion: In the present case, combining ultrasonography, radiography (myelography), and CT was very effective for diagnosing spina bifida, with the subcutaneous abscess inducing spinal cord compression. Additionally, using intraoperative ultrasonographic scanning to evaluate the degree of spinal cord damage can contribute to predicting the postoperative outcome.

Keywords: Abscess, Calf, Computed tomography, Intraoperative spinal ultrasonography, Myelography.

Introduction

As a clinical sign, a swollen back is observed rarely but is associated with various congenital diseases in newborn animals. Spina bifida cystica is one of the most common abnormalities, a disease in which the cysts enveloped within the dura matter protrude through the defects of the spinous process of the vertebrae (Yoshioka *et al.*, 2017). Congenital tumors or tumor-like masses are minor causes of back swellings (Kieck and De Villiers, 1975; Boyd, 1985; Koç *et al.*, 1998; Yoshioka *et al.*, 2017; Toma *et al.*, 2021). Cutaneous

or subcutaneous abscessation is a commonly acquired disease that can also cause a swollen back (Braun *et al.*, 2016).

The swollen back was easily detectable macroscopically and by palpation. However, in newborn or younger animals, it is difficult to differentiate cutaneous or subcutaneous mass lesions such as spina bifida cystica, cellulitis, abscess, tumors, and tumor-like masses macroscopically or by palpation alone (Kieck and De Villiers, 1975; Boyd, 1985; Middleton *et al.*, 1999; Rebsamen *et al.*, 2010; Abouelnasr *et al.*, 2016;

*Corresponding Author: Takeshi Tsuka. Department of Veterinary Clinical Medicine, Joint Department of Veterinary Medicine, Faculty of Agriculture, Tottori University, Tottori, Japan. Email: tsuka@tottori-u.ac.jp



Braun *et al.*, 2016; Yoshioka *et al.*, 2017; Toma *et al.*, 2021). Additionally, the macroscopic observation and palpation cannot allow full evaluation of the various associated abnormalities occurring deeper than the superficial mass; these include osteolytic changes of the underlying bones associated with a subcutaneous tumor or abscess, or the congenital skeletal deformity associated with various types of tumor-like masses (Koç *et al.*, 1998; Middleton *et al.*, 1999; Braun *et al.*, 2016; Yoshioka *et al.*, 2017; Usaki *et al.*, 2024). Imaging is the diagnostic technique for simultaneously evaluating superficial masses and associated deeper diseases. In bovine practice, radiography and ultrasonography can be utilized routinely, and computed tomography (CT) and magnetic resonance imaging (MRI) used as an advanced imaging modality (Chauvet *et al.*, 1994; Struk *et al.*, 2001; Zani *et al.*, 2008; Rebsamen *et al.*, 2010; Braun *et al.*, 2016; Tsuka *et al.*, 2018; Cagnotti *et al.*, 2019; Câmara *et al.*, 2020; Usaki *et al.*, 2024). Radiography is inferior to ultrasonography in terms of the visibility of soft tissue masses as it provides mostly homogenous radiopaque findings for these lesions, causing difficulty in differentiating soft tissue diseases. Ultrasonography is the most valuable imaging modality for evaluating soft tissue masses (Rebsamen *et al.*, 2010; Abouelnasr *et al.*, 2016; Braun *et al.*, 2016; Morita *et al.*, 2019a; Tsuka *et al.*, 2021; Usaki *et al.*, 2024). In diagnosing subcutaneous abscesses, when using ultrasonography and clinical examination, the diagnostic sensitivity and specificity were elevated by 12% and 18%, respectively, compared with those of clinical examination alone (Squire *et al.*, 2005). Soft tissue masses can be partly differentiated based on the ultrasonographic characteristics, despite not being diagnostic: tumor masses appear as mixed consistency and echogenicity; hematomas and abscesses appear as variably echogenic contents enveloped by echogenic capsule structures; cellulitis appears as the thickening and diffuse hyperechogenic changes of the subcutaneous fat tissues, obliterating the fat-dermis interface between the echogenic fat and the dermis, giving the appearance referred to as cobblestoning (Squire *et al.*, 2005; Rebsamen *et al.*, 2010; Abouelnasr *et al.*, 2016; Morita *et al.*, 2019a; Tsuka *et al.*, 2021). Additionally, the accumulation of fluid contents separated by multiple echogenic fibrin septa within the capsule structures is an atypical sign of cellulitis (Squire *et al.*, 2005; Morita *et al.*, 2019a,b). This sign resembles that of chronic abscesses (Abouelnasr *et al.*, 2016). According to a retrospective human report, it is difficult to ultrasonographically differentiate between hematomas and abscesses; hematomas have been misdiagnosed as abscesses in three out of five patients due to false-positive ultrasonography results (Squire *et al.*, 2005). Abscesses can also be mistaken as solid masses on the ultrasonogram in which the debris and semisolid materials are isoechoic to the surrounding tissues, such as the capsular structures (Struk *et al.*, 2001). Thus,

the diagnostic efficacy of ultrasonography is elevated when combined with other diagnostic techniques, such as CT, MRI, and biopsy. CT is superior to radiography in the clear demonstration of the interaction between the soft tissue and bone structures located close to each other in terms of their anatomical position and the spread and diffusion of the lesions (Chauvet *et al.*, 1994; van Hoogmoed *et al.*, 1999; Zani *et al.*, 2008; Yilmaz *et al.*, 2013; Tsuka *et al.*, 2018). CT can provide every-directional and three-dimensional (3D) images through its reconstruction function, visualizing various osseous changes such as osteolytic destructions and bone developments (Tsuka *et al.*, 2016, 2018).

In younger ruminants, the sudden or gradual developments of hindlimb paralysis can be commonly caused by involvements of primary spinal diseases such as syringomyelia and neural tube defect (Testoni *et al.*, 2012; Cagnotti *et al.*, 2019), and spinal injuries due to mechanical compression from the epidural and subcutaneous mass lesions (Rebhun *et al.*, 1984; Middleton *et al.*, 1999; Divers, 2004; Zani *et al.*, 2008; Braun *et al.*, 2016; Panziera *et al.*, 2016). Additionally, trauma-induced vertebral fracture, vertebral osteomyelitis, and discospondylitis can induce spinal cord compression (Divers, 2004; Correa *et al.*, 2013; Tsuka *et al.*, 2016). It is possible for neurological disturbances to arise as one of the minor clinical signs in animals with back swelling, except for meningocele and myelomeningocele (Yoshioka *et al.*, 2017). In terms of the diagnostic efficacy of imaging modalities for primary or secondary spinal diseases, myelography is routinely useful for evaluating the neurological disturbances associated with subcutaneous and epidural masses (Arcomano and Azzoni, 1967; Kieck and De Villiers, 1975; Boyd, 1985; Middleton *et al.*, 1999; Divers, 2004; Zani *et al.*, 2008; Toma *et al.*, 2021). MRI can allow higher resolution soft tissue imaging allowing demonstration of small pathological lesions within the affected spinal cords (Braun *et al.*, 2016; Tsuka *et al.*, 2016). CT can effectively demonstrate the vertebral lesions causing mechanical compression for the spinal cord, despite being inferior to MRI in visibility of the spinal cord (Divers, 2004; Tsuka *et al.*, 2016). Additionally, the myelography technique applies to spinal CT examination in bovine practice (van Hoogmoed *et al.*, 1999; Cagnotti *et al.*, 2019). In comparison with the usual uses of these imaging modalities, ultrasonography has restrictions on its clinical use, because allowing partial demonstration of the spinal cord through the intervertebral window to penetrate ultrasound waves (Testoni *et al.*, 2010, 2012). On the other hand, ultrasonography is very helpful for evaluating the severity of the injured spinal cord, when used during spinal surgery in human patients (Dohrmann and Rubin, 1982; Knake *et al.*, 1983; Quencer *et al.*, 1984; Quencer and Montalvo, 1984; Feldenzer *et al.*, 1986; Falcone *et al.*, 1994; Mak *et al.*, 1996; Ganau *et al.*, 2018), canine cases (Nakayama,

1993; Finn-Bodner *et al.*, 1995; Tanaka *et al.*, 2006; Nanai *et al.*, 2006, 2007; Bonelli *et al.*, 2015) and both canine and feline cases (Galloway *et al.*, 1999). To the best of our knowledge, this technique has not been conducted in previous bovine cases.

The present study included the diagnostic and therapeutic trial for a calf with recurring back swelling and progressive hindlimb paralysis after surgical resection of a protruding, large mass in its back, which was histopathologically diagnosed as a pulmonary choristoma (Usaki *et al.*, 2024). The present study aimed to show the diagnostic efficacy of ultrasonography, myelography, and CT, to investigate the association between the regrown back mass and hindlimb paralysis, and therapeutic decision-making. The study also aims to evaluate the efficacy of intraoperative ultrasonography for observing the degree of spinal damage.

Case Details

A five-month-old female Holstein calf presented with progressive paralysis in both hindlimbs. This occurred after a swelling grew in its back at the same site in which a subcutaneous mass lesion was previously removed. The mass had grown since birth and was removed when the calf was 18 days old. The mass was diagnosed as a pulmonary choristoma by histopathology. Five months transpired between the surgical resection and the exhibition of the signs. The swelling rose approximately 1 cm above the normal skin's surface (Fig. 1A). Under palpation, the swelling had a hard and irregular surface, while the center included soft parts that possibly contained fluid. The animal could stand with human assistance but could not walk. Severe thinning of the thigh muscular layers was evident in both hindlimbs. The muscular layers were also severely wasted in the pelvic region.

At admission, the present case had approximately 100 kg body weight, because of gradual reduction of its body mass. Neurological examination revealed the absence of proprioception and hopping reaction, and weakness of the patellar tendon reflex in both hindlimbs. This animal showed a weak reflex retraction of both hindlimbs when physical pressure was applied to its inter-digital skin. The calf's anal reflex and tail movements were also weak. Neurological examination identified that this animal had developed signs of lower motor neurons. Hematological examination identified leukocytosis (20,700/ μ l, reference range: 6,500–11,500/ μ l) (Table 1) (Morita *et al.*, 2019b). There were no abnormal states of blood biochemistry, except for the high levels of total protein (8.0 g/dl, reference range: 4.7–6.9 g/dl) and albumin (3.9 g/dl, reference range: 2.7–3.7 g/d) (Table 1) (Morita *et al.*, 2019b).

A portable-type ultrasound device (MyLabOne VET, Esaote Corporation, Genova, Italy) was used to observe the internal structures of its back's swelling while scanning subcutaneously at a cranial-caudal longitudinal axis of its back using a 5.0-MHz linear

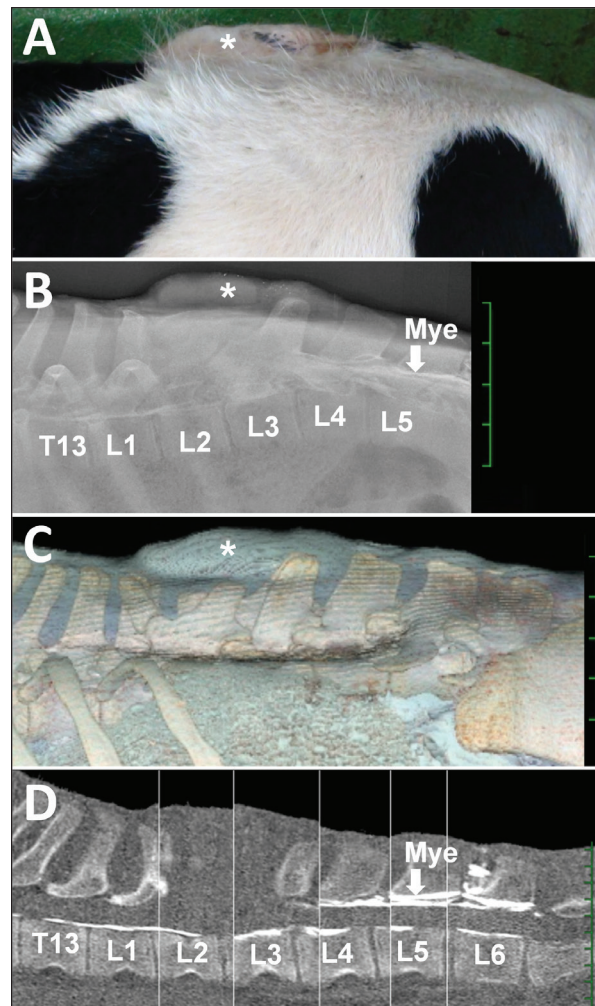


Fig. 1. (A) Photo from the lateral views of a five-month-old female Holstein calf presenting with a swollen back (asterisk). Lateral myelogram (B), 3D CT image (C) and sagittal reconstructed CT image (D) showing the affected area between the thirteenth thoracic vertebra (T13) and the sixth lumbar vertebra (L6), underlying the swollen back (asterisk). Fig. 1D is created by merging several sections obtained from the same CT image because of the slightly curved alignment of the vertebrae when examined. (B) The intradural contrast flow is interrupted at the location of the radiopaque structure of the mass (asterisk) presenting within the space between the second and third lumbar vertebrae (L2 and L3, respectively), revealed by intradural injection of the contrast medium (Mye) between the fifth lumbar vertebra (L5) and L6. Deformation and defects in the spinous process are evident in the first lumbar vertebra (L1) and L2, respectively, compared with the radiopaque shape of the spinous process in the fourth lumbar vertebra (L4). (C) The swollen back region (asterisk) is located between L1 and L3. (D) The dorsal line of the intradural contrast flow from Mye is interrupted at the level of L3, despite the ventral line demonstrated between Mye and T13. The contour of the mass is unclear in the space between L1 and L3.

Table 1. Hematological and serum chemistry states in the present case.

	The present case	Reference values
Red blood cell count ($\times 10^4/\mu\text{l}$)	1,124	853 \pm 101
White blood cell count ($/\mu\text{l}$)	20,700	6,500–11,500
Hemoglobin (g/dl)	13.6	9.8 \pm 1.3
Hematocrit (%)	41.7	30 \pm 5
Total protein (g/dl)	8.0	4.7–6.9
Albumin (g/dl)	3.9	2.7–3.7
Urea nitrogen (mg/dl)	13.4	4.2–17.7
Creatinine (mg/dl)	0.5	0.59–1.28
Aspartate transaminase (U/l)	79	14.9–103.1
γ -glutamyltranspeptidase (U/l)	23	0–91.7
Creatine kinase (U/l)	173	29.8–302.5

transducer. On the ultrasonograms showing the areas cranially and caudally to the swollen mass structures, the spinous process of the first and third lumbar vertebrae (L1 and L3) were seen as hyperechoic, curved lines accompanied by posterior acoustic shadowing (Fig. 2A). However, no echotexture was evident in the spinous process of the second lumbar vertebra (L2). The mass structure fully occupied the space between the spinous process of the L1 and L3. The superficial areas of the mass were ultrasonographically characterized by formations of two large, well-defined compartments of the cystic lesions. At the cranial part of the mass, two superficial cystic lesions were seen as a flat triangle structure, measuring roughly 1.5 and 2 cm in dorsal-ventral height and cranial-caudal length, respectively. The elliptical caudal part had approximately 2 and 3 cm in height and length, respectively. Within the lumens of these two cystic lesions, the contents were commonly anechoic without hyperechoic deposits. One deeper, larger cystic lesion was formed by hyperechoic membranous structures, allowing clear separation from the two superficial cystic lesions. The triple, parallel, echogenic lines running along this lesion defined the deepest part of this lesion. However, the cranial and caudal edges of the deeper cystic lesion were unclear. The height of the deeper cystic lesion could be measured at approximately 3.5 cm. Within the triple-lined structure, visualized as homogeneously hypoechoic, the echogenicity was higher in the dorsal and ventral lines than in the middle line. Based on the ultrasonographic characteristics of the triple-lined structure, the dorsal and ventral hyperechoic lines were the dura membranes, and the thinner middle line was the central canal. Within the echotexture of the spinal cord, the hyperechoic line of the central canal was interrupted. The diameter of the central canal mostly

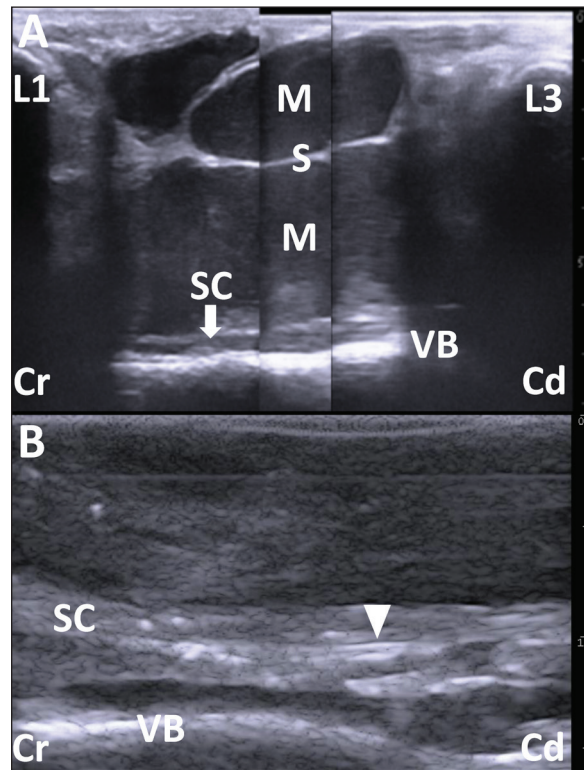


Fig. 2. (A) The ultrasonogram of the mass when scanning longitudinally along the swollen back using a 5.0 MHz linear transducer. This image is created by merging three sections of two ultrasonograms. The hypoechoic capsular mass (M) separated into three parts by the echogenic septal structures (S) is evident within the space between the hyperechoic structures of the spinous process of the first and third lumbar vertebrae (L1 and L3, respectively). The cystic mass extends by 7 cm in depth and is close to the thin, hypoechoic structure of the spinal cord (SC), outlined by the hyperechoic line of the dura mater. The structure of SC runs along the hyperechoic line of the spinal canal's surface between the L1 and L3 (VB). Scale: 1 cm. (B) The intraoperative ultrasonogram of SC is represented as a heterogeneous echogenic structure outlined by the hyperechoic lines. The SC runs along the VB within the hypoechoic background of the saline pool. The double hyperechoic lines (arrowhead) outline the distended central canal. Cr: Cranial; Cd: Caudal. Scale: 5 mm.

kept the same thickness between the L1 and L3, and measured 5–7 mm. The echotexture of the spinal cord was laid peripheral to the thickened, hyperechoic line running across in the cranio-caudal direction. The ventral and osseous surfaces of the vertebral canal were identified between the L1 and L3.

Under ultrasonographic observation, 2–3 mm of yellow mucoid pus was aspirated via a 22-gauge needle (length 38 mm, Terumo Co., Tokyo, Japan) which was inserted into the soft parts of the swelling. The pus tested positive for *Escherichia coli* when examined bacteriologically. The bacteria were resistant to ampicillin, levofloxacin,

and a sulfamethoxazole and trimethoprim combination but were susceptible to cephalosporins.

The animal was examined by radiography and CT under general anesthesia obtained using 2–3% of isoflurane (DS isoflurane, DS Pharma Animal Health Company, Ltd., Osaka, Japan) via an endotracheal tube, inserted after sedation with 0.2 mg/kg xylazine hydrochloride (Selactar 2%, Bayer Yakuin Ltd., Osaka, Japan). Radiography was conducted using a computed radiography machine (REGIUS Console CS-3, Konica Minolta Healthcare Company Ltd., Tokyo, Japan) with an X-ray condition of 80 kVp, 400 mA, and 0.04 seconds. CT was conducted using a 16-section multidetector scanner (ECLoS; Hitachi, Tokyo, Japan) with X-ray tube settings of 120 kVp, a current of 175 mA, and scanning at a 0.625-mm slice thickness. Before imaging examinations, spinal centesis was performed through the intravertebral space between the fifth and sixth lumbar vertebrae (L5 and L6, respectively) using a 22-gauge spinal needle (length 70 mm, TOP spinal needle, TOP Company Ltd., Tokyo, Japan). The cerebrospinal fluid (CSF) was collected and dropped naturally into a micro-tube, followed by the slow injection of contrast medium (0.2 ml/kg, Omnipaque 240 injection, DAIICHI SANKYO Chemical Pharma Company Ltd., Tokyo, Japan).

On the lateral myelogram, the protruding mass was located on the level between the L2 and L3 (Fig. 1B). No radiopaque structure of the spinous process was evident in the L2. The intradural flow of the contrast medium, injected from the intravertebral space between L5 and L6, was interrupted on the dorsal surface of the vertebral canal at the level of the fourth lumbar vertebra (L4). No contrast enhancement was evident in the dorsal spinal tract more cranially than in L4. The location of the contrast interruption corresponded to the mass's area. However, the ventral line of the spinal tract was slightly enhanced up to the level of the twelfth thoracic vertebra. On the 3D-CT corresponding to this lateral myelogram, deformation was evident in the spinous process of the L1 and L3, and in the absence of the spinous process of the L2 (Fig. 1C). The spinous process in the L1 displayed a shortened, forward-bent shape. The L3 had a lower spinous process width and height than the L4. On the reconstructed sagittal CT myelogram, the contrast line along the dorsal surface of the vertebral canal was interrupted cranially to the L4, despite the contrast enhancement of the ventral spinal tract at the level of the thirteenth thoracic vertebra (Fig. 1D). These imaging findings suggested an incomplete spinal cord compression by the subcutaneous cystic mass.

When collected by spinal centesis, the CSF was clear and uncolored, without turbidity or deposits. Cytology of the CSF identified no cellular contents. The CSF concentration of total protein was 18.4 mg/dl. The CSF albumin-globulin ratio was 1.3, as calculated by the CSF percentage, in which albumin, α -globulin,

β -globulin, and γ -globulin were 55.8%, 23.5%, 6.3%, and 14.4%, respectively. No bacteria were isolated from the CSF.

One day after the clinical examination, the animal was anesthetized using the same method as in the imaging examinations. The swollen skin was shaved, disinfected, and injected subcutaneously with lidocaine hydrochloride (xylocaine injection 2%; AstraZeneca K. K., Osaka, Japan). A 20 cm long crescent-shaped skin incision was made along the left margin of the mass (Fig. 3A). Blunt dissection of the subcutaneous tissues led to the exposure of the dark-red surface of the mass, located between the spinous process of the L1 and L3, which could be palpated by the operator's finger (Fig. 3B). The mass could be separated from the adjacent soft tissue layers by dissecting the right-sided border bluntly and using an electric scalpel, while care was taken to prevent the mass's rupture (Fig. 3C). Subsequently, the mass could be separated circumferentially when the dissection was extended from right to left (Fig. 3D). When the operator's finger was inserted deeper than the mass along the left-sided, separated space, adhesion between the dura mater and the ventral mass's surface could be felt. When the mass was carefully lifted, the spinal cord could be seen to rise upward while sticking to the ventral mass's surface (Fig. 3E). The adhesion could be released by carefully separating the fibrous connective tissues that had formed between the dura mater and the ventral mass's surface while the mass was brought upward. A disposable ultrasound probe cover (Echo Probe Cover II, Fuji Medical Company, Ltd., Tokyo, Japan) was used to observe the spinal cord intraoperatively once it was released from the now-removed mass's compression. The covering of a 10 MHz linear transducer was prepared by pouring an ultrasound gel inside the cover, allowing good attachment between the cover's inner surface and the transducer's surface. The covered transducer was inserted into the space of the removed mass, which had been filled with hot sterile saline water (Fig. 3F). Ultrasonographically, the spinal cord presented as a heterogeneous echogenic structure outlined by hyperechoic lines running within the hypoechoic background of the saline pool (Fig. 2B). The hyperechoic line of the central canal was interrupted and partly distended. Double hyperechoic lines outlined the distended central canal. The width of the spinal cord measured 3.4–4.2 mm on the same ultrasonogram. After continuous lavage into the space of the removed mass with saline fluid, the muscular fascia was separated from the surfaces of the both-sided longissimus dorsi muscles at the level of the L1 and L3 (Fig. 3G). The separation of the muscular fascia extended as deeply as possible so it could be used as a muscular flap to shorten the dead space left by the now-removed subcutaneous mass. Both sides of the separated muscular fascia were reversed toward the space of the removed mass and sutured using an absorbable suture material (MAXON; Davis and Geck

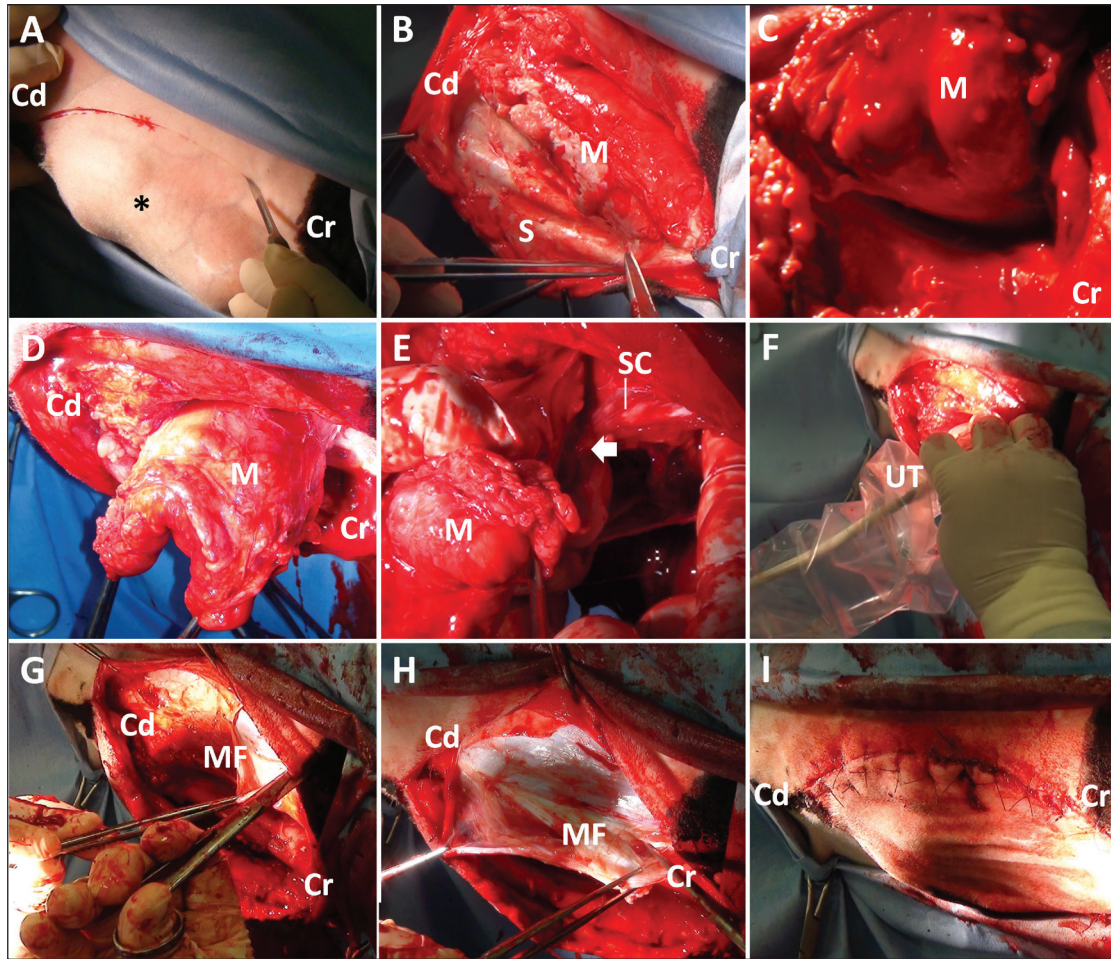


Fig. 3. Photos of the surgical procedure for resecting the subcutaneous back mass. (A) A crescent-shaped skin incision is made along the left margin of the mass (asterisk). (B) A dark-red mass (M) is evident when the subcutaneous structures (S) are dissected bluntly and shifted to the right. (C) The mass (M) is separated from the right-sided surface of the adjacent soft tissue layers. (D) Blunt dissection of the mass (M) is extended from right to left, resulting in circumferential separation. (E) The spinal cord (SC) is seen to adhere (arrow) to the ventral surface of the lifted-up mass (M). (F) The covered ultrasound transducer (UT) is inserted toward the space of the resected mass. (G) The muscular fascia (MF) is separated from the surface of the left-sided longissimus dorsi muscles. (H) Both sides of the separated muscular fascia (MF) are reversed and sutured using absorbable suture material. (I) The macroscopic views after skin suturing. Cr: Cranial; Cd: Caudal.

Inc., Brooklyn, NY) (Fig. 3H). The incised skin was closed using a nylon suture material (Suprylon USP0, Vömel, Gronberg, Germany) (Fig. 3I).

The animal was treated postoperatively with a ten-day subcutaneous injection of an anti-inflammatory drug (0.5 mg, Predonizoron Injection KS, Kyoritsu Seiyaku Company, Osaka, Japan). Over the same ten days, kanamycin (5 mg/kg) or cephazolin (5 mg/kg, cephazolin injection Fujita, Fujita Pharmaceutical Company Ltd., Tokyo, Japan), was administered intramuscularly. These two drugs were alternated. Clinical signs improved slightly, e.g., there was an improvement in the panniculus reflex in the calf's pelvic area and tail movement five days postoperatively. The

animal could sit in a prone position and try to stand up. After that, medication was given irregularly, changing between three antibiotics, including kanamycin (5 mg/kg), a combined penicillin and streptomycin solution (20,000 IU/kg and 25 mg/kg, respectively, intramuscularly, Mycillin, Meiji Seika Pharma Company Ltd, Tokyo, Japan), or enrofloxacin (5 mg/kg subcutaneously, Baytril, Elanco Japan Company Ltd., Tokyo, Japan). However, the daily owner's assistance using a cow lifting device could not contribute to the calf's standing up. Additionally, a pressure wound developed in its hindlimb with severe thinning of the muscular layers. Thus, at the owner's strong request, the animal was euthanized at 38 postoperative days

by intravenous injection of potassium chloride (approximately 2 nmol/kg) under deep anesthesia with intravenous infusions of xylazine hydrochloride (2 mg/kg) and propofol (10 mg/kg). Macroscopic examination during necropsy revealed a defect in the spinous process of the L2. The dura mater adhered firmly to the spinal cord's dorsal surface within this region. The vertebrae between the L3 and L4 looked normal. The skeletal muscles in the hindlimb were severely and diffusely atrophied. Edema was observed extensively within the subcutaneous and intramuscular regions in both hindlimbs. A part of the sciatic nerve looked dark reddish and fragile, suggestive of necrosis, accompanied by necrosis in the adjacent skeletal muscles. Both carpal joints remained flexed due to thickened fibers encapsulating the joints. The axillary, popliteal, sublumbar, and mesenteric lymph nodes were enlarged. There was no macroscopic abnormality in any of the visceral organs.

On the cut surface of the resected mass, a tubular structure was seen to run within the center of the mass parenchyma (Fig. 4A). In the tubular structure, a 2–3 mm thick, white, cartilage-like outer structure formed an empty, rounded lumen measuring approximately 1 cm in diameter, surrounded by this outer structure. This macroscopic feature of this tubular structure resembled bronchi. The mass parenchyma was macroscopically spongiform. The multiple capsular structures, some pus-filled, were present on the spongiform parenchyma. The mass was fixed in 10% neutral buffered formalin and embedded in paraffin wax. Sections were sliced at 4-micrometer thicknesses, stained by hematoxylin and eosin (HE) staining, and observed under a light microscope. The mass consisted of bronchi-like lumens, large arteries with elastic fibers, lymph node, mixed inflammatory cells, and abundant collagen deposits. The lumens were lined by pseudostratified ciliated epithelial cells and supported by cartilage and muscular layers, consistent with a bronchus. Various-sized vasculature, mature adipocytes, peripheral nerve bundles, edema, fibrin depositions, and hemorrhages were found in connective tissues. Infiltration of macrophages, lymphocytes, and granulocytes were multi-focal to coalescing, and a fragment of sutures was seen with multinucleated giant cells (Fig. 4B). Based on these histopathological findings, the lesion was diagnosed as pyogranulomatous inflammation (suture granuloma) in ectopic tissue.

Histopathological examination revealed a loss of their normal histological structure at the locations of the L1 and L2 (Fig. 5). The histopathological abnormalities included extensive necrosis (malacia) in the gray matter, diffuse white matter degeneration with axonal swelling (spheroids), and gliosis and scarring of the dorsal part of the spinal cord, including the dorsal funiculus (Fig. 4C, D). The dura mater was thickened diffusely due to fibrous scar tissue formation. Based on clinical and histopathological examination results, the destructive

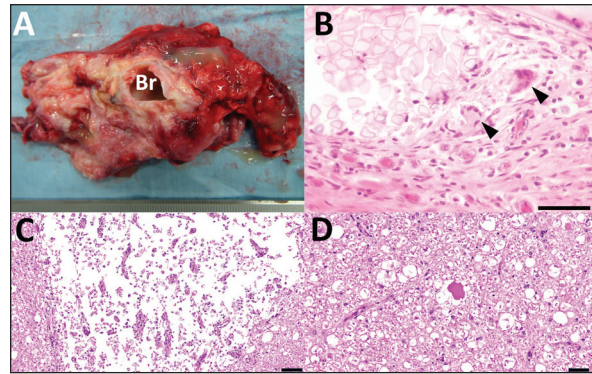


Fig. 4. The cut surface of the resected mass (A) showing a bronchi-like structure in the center of the spongiform parenchyma, including multiple pus-filled capsular structures. (B) Histopathology of a part of the resected mass. Granulomatous inflammation with a cross-section of sutures (left upper side) and some multinucleated giant cells (arrowheads). Capsulation by fibroblasts and neovascularization are also noted. HE, Bar, 50 μ m. Histopathological images of the ventral horn (C) and the ventral funiculus (D) of the first lumbar spinal cord in the specimen obtained at autopsy. (C) Extensive necrosis (malacia) is seen in the gray matter, where no neuron is observable, with infiltration of fat granule cells. HE. Bar, 100 μ m. (D) Swelling of the axon (spheroid) and vacuolization in the myelin sheath are seen. HE. Bar, 50 μ m.

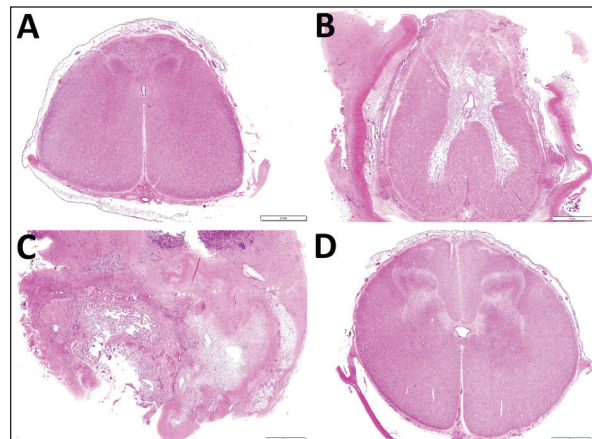


Fig. 5. Transverse section images of the spinal cords at the locations of the thirteenth thoracic vertebra (A) and the first, second and fourth lumbar vertebrae (B, C and D, respectively). (A) Degeneration of the white matter is seen diffusely in the dorsal funiculus and sporadically in the ventral funiculus and the lateral funiculus. (B) Extensive malacia is seen within the gray matter. (C) The spinal cord's structure is destroyed due to extensive malacia with fibrous scar formation. (D) Degeneration of the white matter is mild. Bar, 2 mm.

changes of the gray matter accompanied by neuron loss were considered to contribute to the irreversible development of hindlimb paralysis. The degenerative

changes within the white matter might also be a secondary change.

Discussion

The present case had a subcutaneous abscessation in its back, derived from the residual tissues of pulmonary choristoma following surgery. The origin of the abscessation was evident based on the macroscopic view of the resected mass, including bronchi-like structures in the cut surface (Canpolat and Eröksüz, 2007; Kılıç et al., 2015; Usaki et al., 2024). Complete resection is commonly required to prevent regrowth in performing surgery for animals with congenital mass lesions such as choristoma and hamartoma (Tsuka et al., 2018; Usaki et al., 2024). In the present case, the formation of the subcutaneous mass could have been caused by a suture-induced suppurative reaction. When resecting the calf's protruding mass at 18 days old, silk suture material remained within the surgical wound to close the large feeding vessels. Silk is a natural material obtained from silkworm protein filaments and is slowly absorbed by proteolytic degradation within two years (Yilmaz et al., 2013). Though it has excellent handling qualities and good knot-holding properties, this material can potentially induce an allergenic capillary reaction (Yilmaz et al., 2013). Additionally, based on macroscopic evidence, such as purulent discharge and cystic formation, and histopathologic evidence, such as various degrees of infectious foci within the mass structures in previous cases with pulmonary choristoma (Kılıç et al., 2015), this structure can become the source of infection (Arcomano and Azzoni, 1967; Yilmaz et al., 2013).

In the present case, the ultrasonographic characteristics of the subcutaneous abscess were the capsular structures, including the anechoic fluid-filled cavities separated by the septal structures. The echogenicity of the abscess's contents seems to be lower depending on the developing abscess's chronicity, leading to content liquefaction (Struk et al., 2001; Abouelnasr et al., 2016). Additionally, the formation of echogenic septal structures can be associated with the abscess's chronicity (Abouelnasr et al., 2016). Doppler ultrasonography can be useful for predicting acute or subacute phases of abscessation because it appears the rich vasculature presenting within the capsular walls of the abscess when developing during these phases (Struk et al., 2001). In the present case, Doppler ultrasonography could identify no sign of blood flow within the capsular walls or septal structures. These ultrasonographic findings suggest the chronic phase of abscessation in the present case. Chronicity in abscessation can be ultrasonographically represented by the hyperechoic spots with acoustic shadowing, if inducing the dystrophic calcification in the walls (Struk et al., 2001). However, this ultrasonographic finding seems difficult to differentiate from those of the tumorous masses accompanying calcification (Morita et al., 2019b).

Despite this evidence indicating subcutaneous abscess in the present case, these ultrasonographic findings could not be differentiated from those of some soft tissue masses; the anechoic contents as the acute phase of hematoma; and the fluid-filled cysts separated by the septal structures in cystic cellulitis (Squire et al., 2005; Abouelnasr et al., 2016; Morita et al., 2019a; Tsuka et al., 2021). Thus, collecting the contents accumulated within this mass was vital to support the ultrasonographic findings. This was done using the centesis technique following ultrasonography. The CTs of abscessation are characterized as the variably thickened capsular structures enveloping the purulent contents with variable CT attenuation dependent on its components; CT attenuation is low for the liquefied debris and high for the proteinaceous or hemorrhagic contents (Struk et al., 2001; Morita et al., 2019b). The high attenuation spots (CT value > 200 Hounsfield units), representing calcification, are meaningful evidence that suggests chronicity in abscessation, despite the difficulty in differentiating calcification within the tumor mass (Struk et al., 2001; Morita et al., 2019b). In the present case, the accumulated contents could not be distinguished in CTs from the wall structures, despite the mass being filled with liquid pus. In the present case, ultrasonography and myelography, followed by CT myelography, were successfully utilized to obtain the diagnostic evidence. This evidence found that the subcutaneous abscess could contribute to spinal cord compression via a congenital defect of the spinous process. An ultrasound transducer with a lower frequency should be used to detect the subcutaneous mass's invasion into deeper structures, including the spinal cord, because the higher frequency of ultrasound can contribute to higher resolution images of superficial mass lesions, but cause poor visibility of the deeper structures (Squire et al., 2005). The ultrasound frequency in the transducer used for the previous calves with congenital spinal deformities was between 6 and 10 MHz (Testoni et al., 2010, 2012). An ultrasound frequency of 5 to 7.5 MHz was required for the atlanto-occipital space of adult cattle (Braun and Attiger, 2016). Ultrasonographic visibility of the spinal cord within the cranial lumbar or thoracic vertebrae is commonly poor. This is due to the extended distance between the skin and vertebral canal, dependent on the longer spinous process, compared with the caudal parts of the lumbar vertebrae and cranial parts of the cervical vertebrae, for which ultrasonography can allow demonstration of the spinal cords (Testoni et al., 2010, 2012; Braun and Attiger, 2016). Thus, a lower ultrasound frequency (<6 MHz) may be required for these regions, despite this ultrasound level not always allowing visualization of the spinal cord (Testoni et al., 2010, 2012). Longitudinal ultrasonography of the spinal cord on the levels of cervical and lumbar vertebrae can provide the normal appearance of the hypoechoic spinal cord lined by the hyperechoic dura

mater, along the center of which the hyperechoic line of the central canal (Testoni *et al.*, 2012; Braun and Attiger, 2016). The spinal cord's echotextures are interrupted by the extremely hyperechoic structures of the dorsal surfaces of the vertebrae (Testoni *et al.*, 2012). On the ultrasonogram in the present case, when scanning the swollen back longitudinally, the spinal cord could be observed over the entire layer at approximately 7 cm depth, at the level of L2 and L3. The defects in the vertebral laminae and the spinous process can be a good window, allowing penetration of ultrasound waves generated from the ultrasound transducer applied to the back (Hudson *et al.*, 1998). However, the pathological defect of the vertebral laminae was too small to demonstrate the spinal cord compression associated with the subcutaneous mass when scanning on the swollen surface of the skin (Braun *et al.*, 2016). Even if presenting no congenital defects in the vertebral laminae and spinous process, percutaneous ultrasonographic scanning may provide diagnostic evidence of spinal cord compression in animals with progressive back abscessations, inducing bone destruction of the underlying vertebrae (Correa *et al.*, 2013; Panziera *et al.*, 2016). In the present case, longitudinal spinal ultrasonography could not identify the common ultrasonographic signs of spinal cord compression, such as an extended anechoic central canal surrounded by a hyperechoic dura-arachnoid layer, and the decreased thickness of the spinal cord (Testoni *et al.*, 2010, 2012). Myelography was previously utilized to confirm the association between the spinal cord and subcutaneous back masses such as spina bifida cystica and lipoma (Kieck and De Villiers, 1975; Boyd, 1985; Zani *et al.*, 2008; Toma *et al.*, 2021). On the myelogram, the flow's interception of the intradural contrast medium is a common sign at the location of spinal cord compression (Koç *et al.*, 1998). In the present case, CT myelography allowed the identification of the mechanical compression of the spinal cord due to the weight of the adjacent mass based on the interception of the enhanced lines representing the intradural flows at the affected level. This finding suggests the etiology of the animal's progressive paralysis of its hindlimb, associated with the back mass's growth (Koç *et al.*, 1998). Additionally, the 3D-CT could be utilized for evaluating the etiology and surgical planning, because clarifying the location of the defected spinous process corresponds to the area of the intercepted, enhanced line of the spinal cord on the sagittal reconstructed CT myelography.

When using myelography followed by CT in the present case, no leaking of the contrast medium was evident in the spinal cord between L1 and L3. The CSF examination was very helpful in supporting the results obtained from myelography, which indicated there was no communication between the subcutaneous mass and the underlying spinal cord (Chauvet *et al.*, 1994; Struk *et al.*, 2001; Zani *et al.*, 2008; Tsuka *et al.*,

2018; Câmara *et al.*, 2020). The colorless and non-turbid appearance of CSF was normal, as opposed to the cloudy CSF in various colors commonly found in specimens of suppurative meningitis and abscesses (Câmara *et al.*, 2020). The laboratory CSF data, such as low CSF concentration of total protein, fewer cell contents, and no bacterial isolation, also indicated there was no extension of infection to the spinal cord in the affected region (Zani *et al.*, 2008; Câmara *et al.*, 2020). Increased CSF concentration of protein is partly sensitive to the involvements of epidural or extradural mass causing spinal cord compression (Rebhun *et al.*, 1984). The myelography and CSF results could predict the complete resection of the subcutaneous mass extended between the skin's surface and the defective vertebral laminae due to the release of the adhesion between the mass and the spinal cord.

Surgical resections of the lesions located subcutaneously result in favorable outcomes in most affected calves (Chauvet *et al.*, 1994; Canpolat and Eröksüz, 2007). However, surgery for resecting subcutaneous masses is challenging; there can be neurological disturbance via defect or destruction in the vertebral bones, resulting in a high probability that the treated animals have a poor quality of life after surgery (Koç *et al.*, 1998; Correa *et al.*, 2013). The poor therapeutic outcome seems to depend on the interval between the onset of clinical signs and treatment, including medication with steroid drugs and laparotomy; 15 days is estimated as the recommended interval (Zani *et al.*, 2008). In delaying therapy, degenerative myelopathy commonly develops from spinal cord compression damage inflicted by epidural or subcutaneous masses, and congenital or degenerative vertebral abnormality (Zani *et al.*, 2008; Braun *et al.*, 2016; Panziera *et al.*, 2016). The higher severity of the compression of the involved spinal cord seems to depend on the increasing size of the causative mass. In large animals, one previous equine report described the surgical repair of spina bifida-associated meningocele, although there are many bovine surgical reports for meningoencephalocele via various pathological skull defects (van Hoogmoed *et al.*, 1999; Ohba *et al.*, 2008). Based on these surgical results, the postoperative prognosis seems to become poor depending on the size of the pathological defects (van Hoogmoed *et al.*, 1999; Ohba *et al.*, 2008). In human medicine, the common surgical procedure for myelomeningocele is the removal of the malformed sac, followed by reconstruction of the dural sac using a commercial artificial dura mater; this creates a barrier between the vertebral canal and the peripheral structures and leads to normal CSF flow (Caldarelli and Di Rocco, 2008). In the present case, it was impossible to completely close the dead space left after removing the mass because of its large size; nevertheless, the dura matter was preserved as there was no invasion from the abscess.

Intraoperative uses of spinal ultrasonography have been developed in human medicine using a 3.5–7.5

MHz transducer covered with a sterile globe and sheath (Dohrmann and Rubin, 1982; Knake *et al.*, 1983; Quencer and Montalvo, 1984; Quencer *et al.*, 1984; Feldenzer *et al.*, 1986; Falcone *et al.*, 1994; Ganau *et al.*, 2018). A saline pool procedure—scanning the spinal cord within a surgical site filled with a sterile saline solution—has been used in most of the previous human and veterinary reports, and our scanning method is identical (Knake *et al.*, 1983; Quencer and Montalvo, 1984; Quencer *et al.*, 1984; Feldenzer *et al.*, 1986; Nakayama, 1993; Falcone *et al.*, 1994; Finn-Bodner *et al.*, 1995; Mak *et al.*, 1996; Galloway *et al.*, 1999; Tanaka *et al.*, 2006; Nanai *et al.*, 2006, 2007; Bonelli *et al.*, 2015; Ganau *et al.*, 2018). The saline bath is useful to avoid direct contact of the applied transducer with the spinal cord (Ganau *et al.*, 2018). The normal longitudinal echotexture of the spinal cord is a homogenous hypoechoic structure outlined as hyperechoic within the anechoic fluid contents, including hyperechoic floating bubbles (Quencer and Montalvo, 1984). The central canals are normally represented by hyperechoic lines of various widths running along the center of the spinal cord or are invisible (Quencer and Montalvo, 1984). When compared to normal spinal echotexture, the pathological structures of the spinal cords can be well identified on intraoperative spinal ultrasonograms; a variety of size, shape, and echogenicity in the intraspinal mass lesions can allow differentiation of the cysts, tumors, and small intramedullary foci associated with spinal centesis (Dohrmann and Rubin, 1982; Knake *et al.*, 1983; Quencer *et al.*, 1984). Previous human reports examined the therapeutic efficacy of spinal ultrasonography used during laparotomy, followed by surgical resection of epidural abscess; this technique could provide effective information on the masses, such as their locations and anteroposterior extensions, and degrees of compression that narrow and deform the spinal cords (Feldenzer *et al.*, 1986; Mak *et al.*, 1996; Ganau *et al.*, 2018). The extended central canal can be created by compression from intraspinal or epidural masses (Dohrmann and Rubin, 1982). These ultrasonographic findings are helpful for the intraoperative planning and subsequent removal of the masses (Feldenzer *et al.*, 1986; Mak *et al.*, 1996). Additionally, the real-time images obtained from this technique are useful for assisting needle biopsy, drainage, and shunt placement (Knake *et al.*, 1983; Quencer *et al.*, 1984; Feldenzer *et al.*, 1986; Mak *et al.*, 1996; Morita *et al.*, 2019b). Intraoperative scanning is very useful for evaluating surgical achievement of spinal decompression and retropulsion after removing epidural masses (Quencer *et al.*, 1984; Feldenzer *et al.*, 1986; Ganau *et al.*, 2018). In the previous canine and feline cases, ultrasonography was also used for intraoperative identification of the pathological regions of the spinal cords while scanning through an opening of the vertebral lamina created with laminectomy for surgical decompression in intravertebral disc herniation and Wobbler syndrome,

and surgical resection in spinal arachnoid cysts and various spinal tumors (Nakayama, 1993; Galloway *et al.*, 1999; Nanai *et al.*, 2006; Bonelli *et al.*, 2015). In small animals, the ultrasound frequency of the probe used for intraoperative spinal ultrasonography varied between 5 and 15 MHz (Nakayama, 1993; Finn-Bodner *et al.*, 1995; Galloway *et al.*, 1999; Tanaka *et al.*, 2006; Nanai *et al.*, 2006, 2007; Bonelli *et al.*, 2015). The recommended ultrasound frequency is between 7.5 and 12.0 MHz for demonstration of small-sized structures of the spinal cord in small animals (Hudson *et al.*, 1998). Abnormal echotexture of the affected spinal cords includes an increased echogenicity in the spinal cord affecting intraparenchymal hemorrhage, and the diffuse or focal hyperechoic changes in the trauma-induced injured spinal cord (Finn-Bodner *et al.*, 1995; Hudson *et al.*, 1998). Well-defined, hyperechoic lesions of the swollen spinal cords accompanying with disruption and loss of the central canal's line can represent intraspinal mass formation (Hudson *et al.*, 1998; Nanai *et al.*, 2006, 2007; Bonelli *et al.*, 2015). In the present case, the abnormal echotexture of the spinal cord could suggest a severe spinal damage, when scanning using ultrasonography through the defected vertebral laminae and spinous process after removal of the mass. In human patients, the degree of spinal damage after removing the causative lesions can predict postoperative clinical improvements (Quencer *et al.*, 1984; Feldenzer *et al.*, 1986; Ganau *et al.*, 2018). Spinal cord compression can induce posttraumatic myelopathy and myelomalacia, resulting in poor postoperative course after spinal decompression (Nakayama, 1993; Falcone *et al.*, 1994; Tanaka *et al.*, 2006). Posttraumatic myelopathy is represented as a heterogenous pattern of spinal cord's echogenicity together with the formation of small microcysts (Falcone *et al.*, 1994). Echotexture of myelomalacia seems to be characterized by a mixture of the echogenic changes within the affected spinal cord including an unclear central canal's line (Nakayama, 1993; Tanaka *et al.*, 2006). Doppler ultrasonography helped identify intraspinal mass invasion and judge decompression due to pulsatile microcirculation (Hudson *et al.*, 1998; Tanaka *et al.*, 2006; Nanai *et al.*, 2006, 2007). Lack of vascularization within the compressed spinal cord may lead to the diagnosing of myelomalacia (Bonelli *et al.*, 2015). Thus, Doppler ultrasound scanning would be required in intraoperative spinal ultrasonography for the bovine case.

The present study found the spinal cord can be demonstrated ultrasonographically in calves, when applied percutaneously to the skin surface of thoracolumbar regions, if defects in the vertebral laminae and spinous process are involved. During surgery on the back, which can lead to exposure of the spinal cord, ultrasonography of the exposed spinal cord via the surgical opening is very helpful for evaluating the degree of damage.

Acknowledgment

None.

Conflict of interest

The authors declare that there is no conflict of interest.

Authors' contributions

TT supervised, performed diagnosis and surgery, reviewed the literature, and prepared the manuscript. NU and MH performed postoperative therapy. YO performed surgery. YM performed anesthesia during surgery. TT examined CSF. YS and TM performed a pathological examination for the specimen obtained at surgery. MT, TI, MK, and NY performed pathological examination for the specimen obtained at necropsy. All authors read and approved the final manuscript.

Funding

This report received no specific grant from any funding agency in the public, commercial, or not-for-profit sectors.

Data availability

The authors confirm that the data supporting the findings of this study are available within the article.

References

- Abouelnasr, K., EL-Shafaey, E.S., Mosbah, E. and EL-Khodery, S. 2016. Utility of ultrasonography for diagnosis of superficial swellings in buffalo (*Bubalus bubalis*). *J. Vet. Med. Sci.* 78, 1303–1309.
- Arcomano, J.P. and Azzoni, A.A. 1967. Intralobar pulmonary sequestration and intralobar enteric sequestration associated with vertebral anomalies. *J. Thorac. Cardiovasc. Surg.* 53, 470–476.
- Bonelli, M.A., Tudury, E.A., Santos, C.R.O., Araújo, B.M., Diogo, C.C., Silva, A.C. and Costa, F.S. 2015. Intraoperative ultrasonography of the vertebral canal in dogs. *Arq. Bras. Med. Vet. Zootec.* 67, 655–663.
- Boyd, J.S. 1985. Unusual case of spina bifida in a Friesian cross calf. *Vet. Rec.* 116, 203–205.
- Braun, U. and Attiger, J. 2016. Ultrasonographic examination of the spinal cord and collection of cerebrospinal fluid from the atlanto-occipital space in cattle. *Vet. Clin. North Am. Food Anim. Pract.* 32, 109–118.
- Braun, U., Suarez, J., Gasparini, S., Warislohner, S. and Dennler, M. 2016. Magnetic resonance imaging in a lamb with compression of the thoracic spinal cord by an abscess. *Schweiz. Arch. Tierheilkd.* 158, 573–577.
- Cagnotti, G., Sammartano, F., Bertone, I., Capucchio, M.T., Nicola, I., Sacchi, P., Bellino, C. and D'Angelo, A. 2019. Imaging and genetic investigations of neural tube defect in a calf: case report and review of the literature. *J. Vet. Diagn. Invest.* 31, 228–234.
- Caldarelli, M. and DiRocco, C. 2008. Myelomeningocele primary repair surgical technique. In *Spina bifida: management and outcome*. Eds., Ozek, M.M., G. Cinalli and W.J. Maixner. New York, NY: Springer, pp: 143–155.
- Câmara, A.C.L., Gonzaga, M.C., Ziober, T.M., Queiroz, C.R.R., Fino, T.C.M., Castro, M.B., Borges, J.R.J. and Soto-Blanco, B. 2020. Cerebrospinal fluid analysis in 58 ruminants showing neurological disorders. *Pesq. Vet. Bras.* 40, 346–354.
- Canpolat, İ. and Eröksüz, Y. 2007. Pulmonary sequestration and bronchogenic cyst in a calf. *F. Ü. Sağ. Bil. Derg.* 21, 281–284.
- Chauvet, A.E., Lipsitz, D., Burek, K. and Bailey, C.S. 1994. Pulmonary choristoma in a calf. *Can. Vet. J.* 35, 441–442.
- Correa, C.E., Moeller, Jr. R.B., Adaska, J.M., Clothier, K.A. and Blanchard, P.C. 2013. Pathology in practice. Soft tissue abscesses and vertebral osteomyelitis attributable to *N farcinica* infection in 2 calves. *J. Am. Vet. Med. Assoc.* 242, 1075–1077.
- Divers, T.J. 2004. Acquired spinal cord and peripheral nerve disease. *Vet. Clin. North. Am. Food Anim. Pract.* 20, 231–242.
- Dohrmann, G.J. and Rubin, J.M. 1982. Intraoperative ultrasound imaging of the spinal cord: syringomyelia, cysts and tumors—a preliminary report. *Surg. Neurol.* 18, 395–399.
- Falcone, S., Quencer, R.M., Green, B.A., Patchen, S.J. and Post, M.J. 1994. Progressive posttraumatic myelomalacic myelopathy: imaging and clinical features. *Am. J. Neuroradiol.* 15, 747–754.
- Feldenzer, J.A., Waters, D.C., Knake, J.E. and Hoff, J.T. 1986. Anterior cervical epidural abscess: the use of intraoperative spinal sonography. *Surg. Neurol.* 25, 105–108.
- Finn-Bodner, S.T., Hudson, J.A., Coates, J.R., Sorjonen, D.C., Simpson, S.T., Cox, N.R., Wright, J.C., Garrett, P.D., Steiss, J.E., Vaughn, D.M., Miller, S.C. and Brown, S.A. 1995. Ultrasonographic anatomy of the normal canine spinal cord and correlation with histopathology after induced spinal cord trauma. *Vet. Radiol. Ultrasound.* 36, 39–48.
- Galloway, A.M., Curtis, N.C., Sommerlad, S.F. and Watt, P.R. 1999. Correlative imaging findings in seven dogs and one cat with spinal arachnoid cysts. *Vet. Radiol. Ultrasound.* 40, 445–452.
- Ganau, M., Syrmos, N., Martin, A.R., Jiang, F. and Fehlings, M.G. 2018. Intraoperative ultrasound in spine surgery: history, current applications, future developments. *Quant. Imaging Med. Surg.* 8, 261–267.
- Hudson, J.A., Finn-Bodner, S.T. and Steiss, J.E. 1998. Neurosonography. *Vet. Clin. North Am. Small Anim. Pract.* 28, 943–972.
- Kieck, C.F. and De Villiers, J.C. 1975. Subcutaneous lumbosacral lipomas. *S. Afr. Med. J.* 49, 1563–1566.
- Kılıç, E., Yayla, S., Beytut, E., Baran, V. and Ermutlu, C.Ş. 2015. Subcutaneous ectopic lung in the

- cervical region of a calf—a case report. *Vet. Arhiv.* 85, 701–709.
- Knake, J.E., Chandler, W.F., McGillicuddy, J.E., Gabrielson, T.O., Latack, J.T., Gebarski, S.S. and Yang, P.J. 1983. Intraoperative sonography of intraspinal tumors: initial experience. *Am. J. Neuroradiol.* 4, 1199–1201.
- Koç, Y., Ogurtan, Z., Tuzcu, M., Alkan, F. and Ciftci, M.K. 1998. Heterotypic pulmonary anomaly in paralumbar region of a calf. *Vet. Bil. Derg.* 14, 151–154.
- Mak, K.H., Au, K.K., Fung, K.Y. and Chan, Y.W. 1996. Spinal epidural abscess: a report of nine cases and the use of intra-operative ultrasonography. *Aust. N. Z. J. Surg.* 66, 287–290.
- Middleton, J.R., Valdez, R., Britt, L.G., Parish, S.M. and Tyler, J.W. 1999. Progressive hindlimb paraparesis in a goat associated with a vascular hamartoma. *Vet. Rec.* 144, 264–265.
- Morita, Y., Sugiyama, S. and Tsuka, T. 2019a. Ultrasound images associated with snakebites in a Japanese Black calf. *J. Anim. Sci. Res.* 3:10. doi:10.16966/2576-6457.127.
- Morita, Y., Sugiyama, S., Tsuka, T., Okamoto, Y., Morita, T., Sunden, Y. and Takeuchi, T. 2019b. Diagnostic efficacy of imaging and biopsy methods for peritoneal mesothelioma in a calf. *BMC Vet. Res.* 15, 461.
- Nakayama, M. 1993. Intraoperative spinal ultrasonography in dogs: normal findings and case-history reports. *Vet. Radiol. Ultrasound.* 34, 264–268.
- Nanai, B., Lyman, R. and Bichsel, P. 2006. Intraoperative use of ultrasonography during continuous dorsal laminectomy in two dogs with caudal cervical vertebral instability and malformation (“Wobbler syndrome”). *Vet. Surg.* 35, 465–469.
- Nanai, B., Lyman, R. and Bichsel, P.S. 2007. Use of intraoperative ultrasonography in canine spinal cord lesions. *Vet. Radiol. Ultrasound.* 48, 254–261.
- Ohba, Y., Iguchi, T., Hirose, Y., Takasu, M., Nishii, N., Maeda, S. and Kitagawa, H. 2008. Computer tomography diagnosis of meningoencephalocele in a calf. *J. Vet. Med. Sci.* 70, 829–831.
- Panziera, W., Rissi, D.R., Galiza, G.J.N., Giaretta, P.R., Bianchi, R.M., Bazzi, T. and Barros, C.S.L. 2016. Pathology in practice: Spinal cord compression associated with vaccine granulomas in 2 calves. *J. Am. Vet. Med. Assoc.* 249, 483–485.
- Quencer, R.M. and Montalvo, B.M. 1984. Normal intraoperative spinal sonography. *Am. J. Roentgenol.* 143, 1301–1305.
- Quencer, R.M., Montalvo, B.M., Green, B.A. and Eismont, F.J. 1984. Intraoperative spinal sonography of soft tissue masses of the spinal cord and spinal canal. *Am. J. Roentgenol.* 143, 1307–1315.
- Rebhun, W.C., deLahunta, A., Baum, K.H., King, J. and Roth, L. 1984. Compressive neoplasms affecting the bovine spinal cord. *Compend. Contin. Educ. Pract. Vet.* 6, S396–S400.
- Rebsamen, E., Gygax, D., Dennler, M., Jud, R. and Kummer, M. 2010. External infiltrating lipoma in a two-week-old foal: computed tomographic evaluation for the assessment of the extension and invasiveness of the tumour. *Equine Vet. Educ.* 22, 602–607.
- Squire, B.T., Fox, J.C. and Anderson, C. 2005. ABCESS: Applied bedside sonography for convenient evaluation of superficial soft tissue infections. *Acad. Emerg. Med.* 12, 601–606.
- Struk, D.W., Munk, P.L., Lee, M.J., Ho, S.G. and Worsley, D.F. 2001. Imaging of soft tissue infection. *Radiol. Clin. North. Am.* 39, 277–303.
- Tanaka, H., Nakayama, M. and Takase, K. 2006. Intraoperative spinal ultrasonography in two dogs with spinal disease. *Vet. Radiol. Ultrasound.* 47, 99–102.
- Testoni, S., Pria, A.D. and Gentile, A. 2010. Imaging diagnosis—cerebellar displacement and spina bifida in a calf. *Vet. Radiol. Ultrasound.* 51, 162–164.
- Testoni, S., Mazzariol, S., Daniele, D.P. and Gentile, A. 2012. Ultrasonographic diagnosis of syringohydromyelia and segmental hypoplasia of the lumbar spinal cord in a calf. *J. Vet. Intern. Med.* 26, 1485–1489.
- Toma, H.S., Barreto, J.V.P., Amude, A.M., Toma, C.D.M., Carvalho, A.M., Cabral, L.S., Munhoz, T.C.P., Pertile, S.F.N. and Filho, L.F.C.C. 2021. First occurrence of Arnold Chiari type II malformation and associated abnormalities in a Gir calf produced in vitro from Brazil—case report. *Arq. Bras. Med. Vet. Zootec.* 73, 916–922.
- Tsuka, T., Yamamoto, N., Saneshige, M., Morita, T., Sunden, Y., Murahata, Y., Azuma, K., Osaki, T., Ito, N., Okamoto, Y. and Imagawa, T. 2016. Computed tomographic images of discospondylitis in a calf. *J. Vet. Med. Sci.* 77, 1689–1691.
- Tsuka, T., Okamoto, Y., Yamamoto, N., Hayashi, K., Morita, T., Sunden, Y., Murahata, Y., Azuma, K., Osaki, T., Ito, N. and Imagawa, T. 2018. Unilateral rostral mandibulectomy for gingival vascular hamartoma in two calves. *J. Vet. Sci.* 19, 582–584.
- Tsuka, T., Okamoto, Y., Osaki, T., Azuma, K., Yamashita, M., Amaha, T., Ito, N., Murahata, Y. and Imagawa, T. 2021. Negative pressure wound therapy with a syringe technique for subcutaneous hematoma in a heifer. *J. Vet. Med. Animal Sci.* 4, 1053.
- Usaki, N., Tsuka, T., Hatanaka, M., Sunden, Y., Imamura, A. and Morita, T. 2024. Case report: Diagnosis and treatment of pulmonary choristoma in a newborn calf. *Front. Vet. Sci.* 10, 1257329.
- van Hoogmoed, L., Yarbrough, T.B., Lecouteur, R.A. and Hornof, W.J. 1999. Surgical repair of a thoracic meningocele in a foal. *Vet. Surg.* 28, 496–500.

- Yilmaz, A., Bektemur, G., Ekinci, G.H., Ongel, E.A., Kavas, M., Haciomeroglu, O., Demir, M. and Burunsuzoglu, B. 2013. Extralobar pulmonary sequestration: a case report. *Monaldi Arch. Chest Dis.* 79, 90–92.
- Yoshioka, K., Ishikawa, A., Sugiyama, M., Nagasao, J. and Kikuchi, M. 2017. A case of a giant mass in the lumbar region of a newborn calf. *Okajimas Folia Anat. Jpn.* 94, 1–6.
- Zani, D.D., Romanò, L., Scandella, M., Rondena, M., Riccaboni, P., Morandi, N., Lombardo, R., Di Giancamillo, M., Belloli, A.G. and Pravettoni, D. 2008. Spinal epidural abscess in two calves. *Vet. Surg.* 37, 801–808.